Chapter 8

Conclusions

This thesis presents a novel approach for linear feature extraction from high-resolution SAR images. The main methods for automatic linear landmark recognition base their whole procedure on edge detection. For this reason, edge detectors constitute the first step of the proposed processing chain.

Depending on the applications, the possibility of computing an analytical threshold, which might be applied on the filtered image to yield a desired PFA in output, could be desirable. For this reason, we evaluated the main statistical filters to accomplish such scope: the RoA [8], the T-test [12] and the W-test [13]. Nevertheless, they are sensitive of the hypothesis underlying their theory. However, respecting the hypothesis of statistical independence among pixels without raise the complexity of the model can be done by a simple image downsampling. Instead, the hypothesis of pixels belonging to the same distribution limits the maximum size of the filtering window. Among all, the RoA edge detector yielded the best results followed in ranking by the T-test and the W-test. Nevertheless, since the RoA and the T-test edge detector need a certain distribution of the data (respectively Gamma and Normal), the W-test can be applied in the cases such hypotheses do not hold. To improve the final performance and reduce the multiple border problems, a weighted version of the RoA can be exploited. However, to keep the possibility of computing an analytical threshold even in such case, a novel statistical model was developed. Even though the presented model approximates the real pdf, which does not have closed form, it fits well the data and its mathematical treatability enables us to exploit the model in different way. For example, throughout the proposed model we found an interesting property of the RoA applied to linear borders: increasing the filtering window length makes raise their detection rate, even on very thin edges. Moreover, analytical computation of the performance varying the number of windows was possible by the proposed model, which also enables a performance improving to be reached on the subsequent linking stage.

Nevertheless, when more complicated models of the backscattering behavior are considered, the proposed statistical filter could not fit such data. In this case, the appropriate filters could involve several parameters whose estimation could be both difficult and time-consuming. In this sense, the simplicity and mathematical treatability of the model is often preferred to formal correctness. For this reason, and to reach a performance improving by a non-linear combination of pixels, the general multiscale linear filtering is investigated. In particular, exploiting different linear filters (Canny [25], Shen-Castan [33], Deriche [35], Paillou [36], and Quadratic Box Spline [27]), we evaluated several methods of scale combinations and automatic thresholding. Our results show how all these filters are good when the noise power is low, and how their performance gets worse on real one-look CSK data.

However, the edge map retrieved by edge detectors can be refined and improved by a subsequent linking stage. For this purpose, we propose to use a modified version of the SEL algorithm [41] that models the linking issue as a shortest path problem (SPP). Actually, the original model was completely modified to solve the loops problem and to allow SEL to be used on the multiplicative noise case. Further in deep, both a parametric (“LR”) and a non-parametric (“Phy”) metric has been proposed to make the method generally applicable. In our experiments LR metrics obtain the best performance and a further improving on the results can be reached by exploiting the model developed as general extension of the RoA edge detector.

The novel algorithm devised to extract linear features (e.g. roads and runways) relies on a modified version of the Hough Transform. In fact, each time a line is vectorized, its contribution is deleted in the transformed domain to dim the corresponding noise. Moreover, most of information that arises from the edge detection step is exploited to drive a correct vectorization. Then, a new approach to find theoretical sound bounds in the Hough Transform discretization has been followed. Surprisingly, the formulas derived with such methods are very near to the signal theory ones and they are tighter than those suggested following the rounding error theory alone [55]. Then, iterating the vectorizing procedure until all pixels are vectorized (even as single point), the object boundaries becomes a composition of linear segments. Next, thanks to a “grow and merge” procedure, even a smooth curve in the road could be recognized as part of “grown line”. Finally, the road is recognized as composition of regions that are limited by symmetric “grown lines” and characterized by a low radar cross section (RCS) and high homogeneous material (low coefficient of variation). The results reported in this thesis confirm the feasibility of this approach for road extraction.

Finally, to improve edge detection performance and approach a higher level of processing, a novel despeckling algorithm is presented. In particular, we have presented a novel anisotropic diffusion filter that manages to combine normally contrasting requirements: reducing noise on homogeneous regions, preserving weak edges, and keeping corners and targets intact (maintaining them as seen in the original image). Moreover, since such filter is a PDE-based filter, no noise model is presupposed so that, in principle, it can be applied to any noise type. We want to emphasize that this last property has a strong impact on its possible application. In fact, no mathematical modeling effort is required (e.g. statistical modeling of both noise and radar reflectivity) to change sensor or data type (e.g. intensity or amplitude). In addition, since the filtered image is a solution of a PDE, many theorems and properties hold for such a solution. Ultimately, visual impressions and performance indexes confirm that our techniques outperforms state-of-the-art filters for SAR image despeckling.

Appendixes

Appendix A

RoA Threshold Computation

In general, the computation of the threshold T needs the inversion of the following equation:

$$P_{FA} = P\{r < T | H_0\} = \int_0^T f_{r|H_0}(r)\, dr = \int_0^T 2\frac{\Gamma(2N\hat{L})}{\Gamma(N\hat{L})^2}\frac{r^{N\hat{L}-1}}{(r+1)^{2N\hat{L}}}\, dr \tag{A. 1}$$

with $\hat{L}$ the estimated number of looks. The **Fisher-Snedecor** pdf $f_{F_{u,v}}(r)$ is the following:

$$f_{F_{u,v}}(r) = \frac{\Gamma\left(\frac{1}{2}u + \frac{1}{2}v\right)}{\Gamma\left(\frac{1}{2}u\right)\Gamma\left(\frac{1}{2}v\right)}\frac{u^{\frac{u}{2}}v^{\frac{v}{2}}r^{\frac{1}{2}(u-2)}}{(ur+v)^{-\frac{1}{2}(u+v)}} \tag{A. 2}$$

so that, changing variables:

$$\begin{cases} a = u/2 \\ b = v/2 \end{cases} \tag{A. 3}$$

we have:

$$\begin{aligned} f_{F_{u,v}}(r) &= \frac{\Gamma(a+b)}{\Gamma(a)\Gamma(b)}\frac{(2a)^a(2b)^b r^{(a-1)}}{(2ar+2b)^{(a+b)}} \\ &= \frac{\Gamma(a+b)}{\Gamma(a)\Gamma(b)}\frac{(2a)^a(2b)^b r^{(a-1)}}{(2a)^{(a+b)}\left(r+\frac{b}{a}\right)^{(a+b)}} \\ &= \frac{\Gamma(a+b)}{\Gamma(a)\Gamma(b)}\left(\frac{b}{a}\right)^b\frac{r^{(a-1)}}{\left(r+\frac{b}{a}\right)^{(a+b)}} \end{aligned} \tag{A. 4}$$

Now, setting $a = b = N\hat{L}$ in Eq. (A. 4) we have:

$$f_{r|H_0}(r) = 2\, f_{F_{u,v}}(r) = \frac{\Gamma(2N\hat{L})}{\Gamma(N\hat{L})^2}\frac{r^{N\hat{L}-1}}{(r+1)^{2N\hat{L}}} \tag{A. 5}$$

that is:

$$P_{FA} = P\{r < T | H_0\} = 2P\{F_{u,v} < T\} \tag{A. 6}$$

Now, relating the **Fisher-Snedecor** cdf with the **Incomplete Beta function** $I_y(b,a)$ [10]:

$$P\{F_{u,v} < T\} = I_y(a,b) \tag{A. 7}$$

where:

$$y = 1 - \frac{b}{b + aT} \tag{A. 8}$$

we have all the variable we need for the inversion. In fact, fixed the desired P_{FA}, the threshold T can be computed throughout the following passages:

- given N and $\hat{L}$ we compute $a = b = N\hat{L}$;
- given the P_{FA} we compute $P\{F_{u,v} < T\} = \frac{P_{FA}}{2}$ (see Eq. (A. 6));
- given a, b and $P\{F_{u,v} < T\}$, we compute y from (A. 7) exploiting the fast inversion method of the **Incomplete Beta function**;
- given y we retrieve the threshold T by manipulating Eq. (A. 8), i.e. exploiting the following equation:

$$T = \frac{by}{a(1-y)} \tag{A. 9}$$

Appendix B

T-test Threshold Computation

The computation of the threshold T needs the inversion of the following equation:

$$P_{FA} = P\{t > T | H_0\} = \int_T^\infty f_{t|H_0}(t)dt = \int_T^\infty 2\frac{\left(1+\frac{t^2}{\hat{\nu}}\right)^{-\left(\frac{\hat{\nu}+1}{2}\right)}}{\sqrt{\hat{\nu}}\,B\left(\frac{1}{2},\frac{\hat{\nu}}{2}\right)}dt \tag{B. 1}$$

we can prove [12], the following relation with the **Fisher-Snedecor** cdf holds:

$$P_{FA} = P\{t > T | H_0\} = P\{F_{u,v} > T^2 \,|\, u = 1, v = \hat{\nu}\} \tag{B. 2}$$

Then, exploiting the following relation [10]:

$$P_{FA} = P\{t > T | H_0\} = I_x\left(\frac{\hat{\nu}}{2},\frac{1}{2}\right) \tag{B. 3}$$

where $I_x\left(\frac{\hat{\nu}}{2},\frac{1}{2}\right)$ is the **Incomplete Beta Fuction**, and the following holds:

$$x = \frac{\hat{\nu}}{\hat{\nu}+T^2} \tag{B. 4}$$

Therefore, we have all the variable we need for the inversion. In fact, fixed the desired P_{FA}, the threshold T can be computed throughout the following passages:

- given $\hat{\nu}$, P_{FA} and resorting to Eq. (B. 3), we compute x exploiting the fast inversion method of the **Incomplete Beta function**;
- given x we retrieve the threshold T by manipulating Eq. (B. 4), i.e. exploiting the following equation:

$$T = \sqrt{\frac{\hat{\nu}(1-x)}{x}} \tag{B. 5}$$

Appendix C

WMW-test Threshold Computation

The computation of the threshold T needs the inversion of the following equation:

$$P_{FA} = \int_{T}^{\infty} f_{W|H_0}(w)dw = \int_{T}^{\infty} 2\frac{1}{\sqrt{2\pi}} e^{-\frac{w^2}{2}} dw \tag{C. 1}$$

it can be proved [10] that, given a r.v. $G \sim N(0,1)$, the following relation holds:

$$P_{FA} = P\{W > T | H_0\} = 2P\{G > T\} \tag{C. 2}$$

Given the symmetry OF Normal pdf we have:

$$2P\{G > T\} = 2P\{G < -T\} = 2\Theta(-T) \tag{C. 3}$$

where $\Theta(T)$ is the Normal cdf. Relating the Normal cdf to the **Complemetary Error function** $erfc(\cdot)$:

$$P_{FA} = 2\Theta(-T) = erfc(x) \tag{C. 4}$$

with:

$$x = T/\sqrt{2} \tag{C. 5}$$

we can exploit the fast inversion algorithm for this last function. Therefore, we have all the variable we need for the inversion. In fact, fixed the desired P_{FA}, the threshold T can be computed throughout the following passages:

- given the P_{FA} we compute x exploiting the fast inversion method of the **Complemetary Error function**;
- given x we retrieve the threshold T by manipulating Eq. (C. 5), i.e. exploiting the following equation:

$$T = x\sqrt{2} \tag{C. 6}$$

Appendix D

Sums of Generic Gamma r.v.s: A Very Accurate Approximation

Given the following r.v.:

$$Y_1 = X_{\Sigma}^{'} + X_{\Sigma}^{''} \sim \Gamma\left(N_1 L, \frac{\sigma_1}{NL}\right) + \Gamma\left(N_2 L, \frac{\sigma_2}{NL}\right) \tag{D. 1}$$

remembering that mean and variance of a generic Gamma r.v. are:

$$\begin{aligned} &X \sim \Gamma(\alpha, \beta) \\ &\mu_X = \alpha\beta \\ &\text{var}[X] = \alpha\beta^2 \end{aligned} \tag{D. 2}$$

and considering the approximation of the sums of generic Gamma r.v.s distributed as a Gamma with mean and variance of the real pdf, we have:

$$\begin{aligned} \mu_{Y_1} &= E[Y_1] = E\left[X_{\Sigma}^{'} + X_{\Sigma}^{''}\right] = E\left[X_{\Sigma}^{'}\right] + E\left[X_{\Sigma}^{''}\right] = \frac{N_1 L\sigma_1}{NL} + \frac{N_2 L\sigma_2}{NL} = \frac{N_1\sigma_1 + N_2\sigma_2}{N} \\ \text{var}[Y_1] &= \text{var}\left[X_{\Sigma}^{'} + X_{\Sigma}^{''}\right] = \text{var}\left[X_{\Sigma}^{'}\right] + \text{var}\left[X_{\Sigma}^{''}\right] = \frac{N_1 L\sigma_1^2}{N^2 L^2} + \frac{N_2 L\sigma_2^2}{N^2 L^2} = \frac{N_1\sigma_1^2 + N_2\sigma_2^2}{N^2 L} \end{aligned} \tag{D. 3}$$

so that the parameters of the resulting Gamma r.v. $Y_1 \sim \Gamma(\alpha_1, \beta_1)$ are:

$$\begin{aligned} \alpha_1 &= \frac{\mu_{Y_1}^2}{\text{var}[Y_1]} = \frac{L(N_1\sigma_1 + N_2\sigma_2)^2}{N_1\sigma_1^2 + N_2\sigma_2^2} \\ \beta_1 &= \frac{\text{var}[Y_1]}{\mu_{Y_1}} = \frac{N_1\sigma_1^2 + N_2\sigma_2^2}{NL(N_1\sigma_1 + N_2\sigma_2)} \end{aligned} \tag{D. 4}$$

Appendix E

Ratio of Generic Gamma r.v.s

The distribution $f_r(r)$ of the ratio between two independent r.v.s $r = Y_1/Y_2$ is given by [8]:

$$f_r(r) = \int_0^{+\infty} f_{Y_1}(ry_2) f_{Y_2}(y_2) y_2 \ \partial y_2 \tag{E. 1}$$

when the r.v.s Y_1 and Y_2 follow a Gamma pdf:

$$\begin{aligned} f_{Y_1}(y_1) &= \frac{{y_1}^{\alpha_1 - 1}}{{\beta_1}^{\alpha_1}\Gamma(\alpha_1)} e^{-\frac{y_1}{\beta_1}} \\ f_{Y_2}(y_2) &= \frac{{y_2}^{\alpha_2 - 1}}{{\beta_2}^{\alpha_2}\Gamma(\alpha_2)} e^{-\frac{y_2}{\beta_2}} \\ f_r(r) &= \int_0^{+\infty} f_{Y_1}(ry_2) f_{Y_2}(y_2) y_2 \ \partial y_2 = \int_0^{+\infty} \frac{(ry_2)^{\alpha_1 - 1}}{{\beta_1}^{\alpha_1}\Gamma(\alpha_1)} e^{-\frac{ry_2}{\beta_1}} \frac{{y_2}^{\alpha_2 - 1}}{{\beta_2}^{\alpha_2}\Gamma(\alpha_2)} e^{-\frac{y_2}{\beta_2}} y_2 \ \partial y_2 \\ &= \frac{r^{\alpha_1 - 1}}{{\beta_1}^{\alpha_1}{\beta_2}^{\alpha_2}\Gamma(\alpha_1)\Gamma(\alpha_2)} \int_0^{+\infty} {y_2}^{\alpha_1 + \alpha_2 - 1} e^{-\frac{(r\beta_2 + \beta_1)y_2}{\beta_1\beta_2}} \ \partial y_2 \end{aligned} \tag{E. 2}$$

so that, changing variables:

$$t = \frac{(r\beta_2 + \beta_1)y_2}{\beta_1\beta_2} \ \Rightarrow \ y_2 = \frac{t\beta_1\beta_2}{(r\beta_2 + \beta_1)} \ \Rightarrow \ \partial y_2 = \frac{\beta_1\beta_2}{(r\beta_2 + \beta_1)} \partial t \tag{E. 3}$$

we have:

$$f_r(r) = \frac{r^{\alpha_1 - 1}}{{\beta_1}^{\alpha_1}{\beta_2}^{\alpha_2}\Gamma(\alpha_1)\Gamma(\alpha_2)} \left(\frac{\beta_1\beta_2}{(r\beta_2 + \beta_1)} \right)^{\alpha_1 + \alpha_2} \int_0^{+\infty} t^{\alpha_1 + \alpha_2 - 1} e^{-t} \ \partial t \tag{E. 4}$$

Remembering the definition of the Gamma function:

$$\Gamma(\alpha_1 + \alpha_2) = \int_0^{+\infty} t^{\alpha_1 + \alpha_2 - 1} e^{-t} \ \partial t \tag{E. 5}$$

replacing it in Eq. (E. 4) and simplifying some terms we have:

$$f_r(r) = \frac{\Gamma(\alpha_1 + \alpha_2)}{\Gamma(\alpha_1)\Gamma(\alpha_2)} \left(\frac{\beta_1}{\beta_2} \right)^{\alpha_2} \frac{r^{\alpha_1 - 1}}{\left(r + \frac{\beta_1}{\beta_2} \right)^{\alpha_1 + \alpha_2}} \tag{E. 6}$$

Now, considering that the r.v. $r_{\min} = \min(Y_1/Y_2 \, , Y_2/Y_1)$ is equivalent to the following r.v.:

$$r_{\min} = \begin{cases} r & r \le 1 \\ \dfrac{1}{r} & r > 1 \end{cases} \tag{E. 7}$$

which is linked to the r.v. $r = Y_1/Y_2$ throughout the graphic in Fig. E.1.

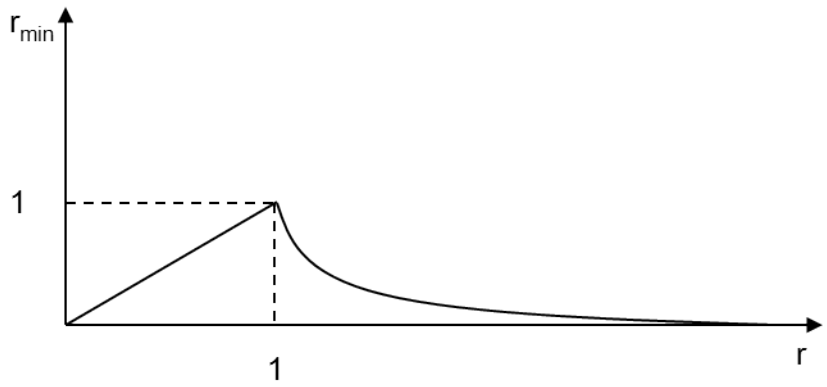

Fig. E.1 - Mathematical link between *r* and r_{min}.

From Fig. E.1 results intuitive that:

$$\begin{aligned} F_{r_{\min}}(r_{\min}) &= P\{r_{\min} \le r_{\min}\} = P\{r \le r_{\min}\} + P\left\{r \ge \frac{1}{r_{\min}}\right\} \\ &= P\{r \le r_{\min}\} + P\left\{\frac{1}{r} \le r_{\min}\right\} = F_r(r_{\min}) + F_{\frac{1}{r}}(r_{\min}) \\ f_{r_{\min}}(r_{\min}) &= \frac{\partial}{\partial r_{\min}}\left[F_{r_{\min}}(r_{\min})\right] = f_r(r_{\min}) + f_{\frac{1}{r}}(r_{\min}) \end{aligned} \tag{E. 8}$$

where we have indicated with $F_x(x)$ the generic cdf. Finally, since the r.v. $1/r = Y_2/Y_1$ is equal to the r.v. $r = Y_1/Y_2$ but with reversed Y_1 and Y_2, we have:

$$\begin{aligned} f_{r_{\min}}(r_{\min}) &= f_r(r_{\min}) + f_{\frac{1}{r}}(r_{\min}) \\ f_{r_{\min}}(r_{\min}) &= \frac{\Gamma(\alpha_1+\alpha_2)}{\Gamma(\alpha_1)\Gamma(\alpha_2)}\left(\frac{\beta_1}{\beta_2}\right)^{\alpha_2} \frac{r_{\min}^{\alpha_1-1}}{\left(r_{\min}+\frac{\beta_1}{\beta_2}\right)^{\alpha_1+\alpha_2}} + \frac{\Gamma(\alpha_1+\alpha_2)}{\Gamma(\alpha_1)\Gamma(\alpha_2)}\left(\frac{\beta_2}{\beta_1}\right)^{\alpha_1} \frac{r_{\min}^{\alpha_2-1}}{\left(r_{\min}+\frac{\beta_2}{\beta_1}\right)^{\alpha_1+\alpha_2}} \\ &= \frac{\Gamma(\alpha_1+\alpha_2)}{\Gamma(\alpha_1)\Gamma(\alpha_2)}\left[\left(\frac{\beta_1}{\beta_2}\right)^{\alpha_2} \frac{r_{\min}^{\alpha_1-1}}{\left(r_{\min}+\frac{\beta_1}{\beta_2}\right)^{\alpha_1+\alpha_2}} + \left(\frac{\beta_2}{\beta_1}\right)^{\alpha_1} \frac{r_{\min}^{\alpha_2-1}}{\left(r_{\min}+\frac{\beta_2}{\beta_1}\right)^{\alpha_1+\alpha_2}}\right] \end{aligned} \tag{E. 9}$$

Appendix F

Properties of the RoA pdf Varying Window and Edge Orientations

The properties of the RoA pdf varying window and edge orientations are:

Property 1 $f_{r_{A_i|A_i}} = f_{r_{B_i|B_i}} \quad \forall i$

Property 2 $f_{r_{A_i|A_j}} = f_{r_{B_i|B_j}} \quad \forall i,j \text{ with } j \neq i$

Property 3 $f_{r_{A_i|B_j}} = f_{r_{B_j|A_i}} \quad \forall i,j$

Property 4 $f_{r_{A_i|B_j}} = f_{r_{A_k|B_j}} \quad \forall i,j,k \text{ with } k \neq i$

The first property states that when a filtering window is applied with the same orientation of the edge, the r.v. $r = \min \{\bar{I}_1/\bar{I}_2, \bar{I}_2/\bar{I}_1\}$ has the same pdf independently for the edge orientation. From Fig. F.1 results clear that r has the same pdf in every case shown in figure since the number of pixels with different scale parameter inside each part of the window is the same (equal to zero).

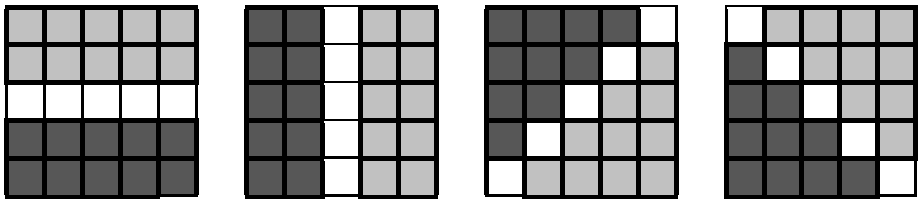

Fig. F.1 - Filtering window with the same orientation of the edge.

The second property states that the r.v. $r = \min \{\bar{I}_1/\bar{I}_2, \bar{I}_2/\bar{I}_1\}$ has the same pdf if the window is orthogonal to the edge. Even in this case (see Fig. F.2), since the number of pixels with different scale parameter inside each part of the window is the same (equal to 4 and 6).

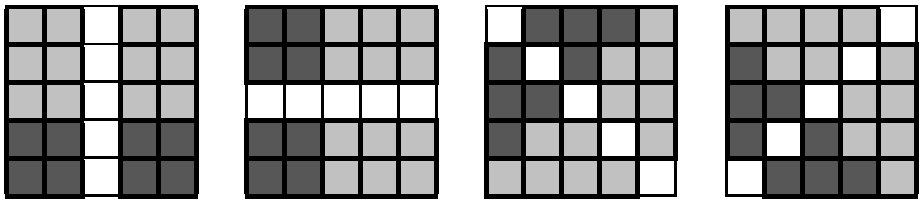

Fig. F.2 - Filtering window orthogonal to the edge.

The third property states that filtering an edge with a window which is neither identical nor orthogonal to the edge orientation may generates the same pdf for some particular cases. For example, it highlights that filtering an edge with orientation 135° with a vertical window gives the same pdf of filtering a vertical edge with a 135° window (see Fig. F.3).

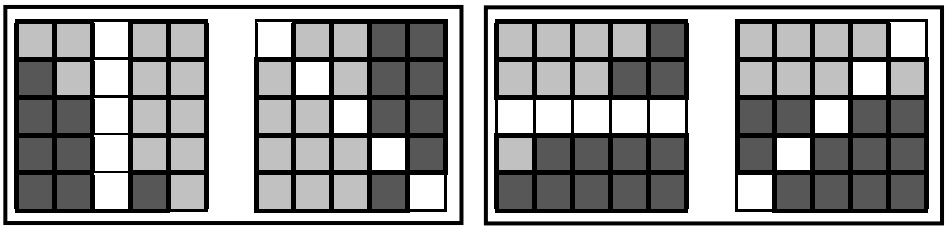

Fig. F.3 - Some examples highlighting the validity of the third property.

The fourth property states that filtering an edge with a window which is neither identical nor orthogonal to the edge orientation may generates the same pdf for some particular cases. For example, it highlights that filtering an edge with orientation 135° with a vertical window gives the same pdf of filtering it with a horizontal window, i.e. a window orthogonal to the former one (see Fig. F.4).

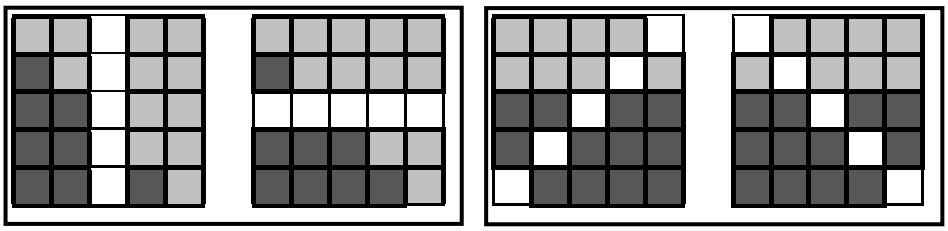

Fig. F.4 - Some examples highlighting the validity of the fourth property.

Appendix G

RoA pdf with a Window Overlapped to a Generic Width Border

Given the formulas reported in Eq. (3.52):

$$\begin{aligned} \alpha_1 &= \frac{L\left(N_1^{(1)}\sigma_1 + N_2^{(1)}\sigma_2\right)^2}{N_1^{(1)}\sigma_1^2 + N_2^{(1)}\sigma_2^2} \quad \beta_1 = \frac{N_1^{(1)}\sigma_1^2 + N_2^{(1)}\sigma_2^2}{NL\left(N_1^{(1)}\sigma_1 + N_2^{(1)}\sigma_2\right)} \\ \alpha_2 &= \frac{L\left(N_1^{(2)}\sigma_1 + N_2^{(2)}\sigma_2\right)^2}{N_1^{(2)}\sigma_1^2 + N_2^{(2)}\sigma_2^2} \quad \beta_2 = \frac{N_1^{(2)}\sigma_1^2 + N_2^{(2)}\sigma_2^2}{NL\left(N_1^{(2)}\sigma_1 + N_2^{(2)}\sigma_2\right)} \end{aligned} \tag{G. 1}$$

Let us consider the configuration in Fig. G.1.

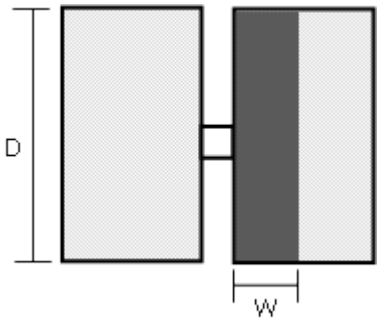

Fig. G.1 - Vertical window with side length *D* overlapped to a border of width *W*.

where σ_1 and σ_2 are the RCS of the background and border respectively, we have:

$$\begin{cases} N_1^{(1)} = N \\ N_2^{(1)} = 0 \\ N_1^{(2)} = DW \\ N_2^{(2)} = N - DW \end{cases} \tag{G. 2}$$

Therefore, the resultant parameters are:

$$\begin{aligned} \alpha_1 &= LN \qquad \beta_1 = \frac{\sigma_1}{NL} \\ \alpha_2 &= \frac{L(DW\sigma_1 + (N-DW)\sigma_2)^2}{DW\sigma_1^2 + (N-DW)\sigma_2^2} \quad \beta_2 = \frac{DW\sigma_1^2 + (N-DW)\sigma_2^2}{NL(DW\sigma_1 + (N-DW)\sigma_2)} \end{aligned} \tag{G. 3}$$

where α_2 and β_2 can be rewritten as:

$$\begin{aligned} \alpha_2 &= L\frac{(C_1)^2}{C_2} = LC_\alpha = L_{Eq} \\ \beta_1 &= \frac{\sigma_1}{NL}\frac{C_1}{C_2} = \frac{\sigma_{Eq}}{NL_{Eq}} \end{aligned} \tag{G. 4}$$

with:

$$\begin{aligned} &R = \sigma_2/\sigma_1 \quad C_\alpha = (C_1)^2/C_2\,; \quad C_1 = WDR + (N - WD); \\ &L_{Eq} = LC_\alpha; \quad C_\beta = C_2/(C_1)^3\,; \quad C_2 = WDR^2 + (N - WD); \end{aligned} \tag{G. 5}$$

so that, by Eq. (3.48) the final pdf becomes:

$$f_r(r) = \frac{1}{B(NL_{Eq}, NL)}\left[\frac{(C_\beta)^{NL_{Eq}} r^{NL_{Eq}-1}}{(r + C_\beta)^{NL_{Eq}+NL}} + \frac{(1/C_\beta)^{NL_{Eq}} r^{NL-1}}{\left(r + \frac{1}{C_\beta}\right)^{NL_{Eq}+NL}}\right] \quad \text{(G. 6)}$$

Appendix H

RoA pdf with Negative Exponential Weights

Indicating with $\bar{I}$ the sample mean of pixels X_i weighted with the coefficients c_i:

$$\bar{I} = \sum_i c_i X_i \tag{H. 1}$$

Presupposing X_i as i.i.d. Gamma r.v.s with mean RCS σ_i and number of looks L:

$$X_i \sim \Gamma\left(L, \frac{\sigma_i}{L}\right) \tag{H. 2}$$

The r.v.s $Y_i = c_i X_i$ due to the multiplication of a Gamma r.v. X_i by the positive constant c_i is distributed as:

$$Y_i \sim \Gamma\left(L, \frac{c_i \sigma_i}{L}\right) \tag{H. 3}$$

Considering the approximation of the sums of generic Gamma r.v.s distributed as a Gamma with mean and variance of the real pdf, we have:

$$\begin{aligned} &\bar{I} = \sum_{i=1}^{N} c_i X_i = \sum_{i=1}^{N} Y_i \\ &\bar{I} \sim \Gamma(\alpha, \beta) \end{aligned} \tag{H. 4}$$

with:

$$\begin{aligned} \alpha\beta &= E\left[\bar{I}\right] = E\left[\sum_{i=1}^{N} Y_i\right] = \sum_{i=1}^{N} E\left[Y_i\right] = \sum_{i=1}^{N} c_i \sigma_i \\ \alpha\beta^2 &= \operatorname{var}\left[\bar{I}\right] = \operatorname{var}\left[\sum_{i=1}^{N} Y_i\right] = \sum_{i=1}^{N} \operatorname{var}\left[Y_i\right] = \sum_{i=1}^{N} \left(c_i \sigma_i\right)^2 / L \end{aligned} \tag{H. 5}$$

so that:

$$\begin{aligned} \alpha &= \frac{E\left[\bar{I}\right]^2}{\operatorname{var}\left[\bar{I}\right]} = \frac{\left(\sum_{i=1}^{N} c_i \sigma_i\right)^2}{\left(\sum_{i=1}^{N} \left(c_i \sigma_i\right)^2 / L\right)} \\ \beta &= \frac{\operatorname{var}\left[\bar{I}\right]}{E\left[\bar{I}\right]} = \frac{\left(\sum_{i=1}^{N} \left(c_i \sigma_i\right)^2 / L\right)}{\sum_{i=1}^{N} c_i \sigma_i} \end{aligned} \tag{H. 6}$$

Now, presupposing the window overlapped to two homogeneous areas with RCS σ_1, σ_2, the RoA operator $r = \bar{I}_1 / \bar{I}_2$ has the following pdf $f_r(r)$:

$$\begin{aligned} r = \frac{\bar{I}_1}{\bar{I}_2} &\sim \frac{\Gamma\left(L \frac{C_\Sigma^2}{C_{\Sigma^2}}, \frac{\sigma_1}{L} \frac{C_{\Sigma^2}}{C_\Sigma}\right)}{\Gamma\left(L \frac{C_\Sigma^2}{C_{\Sigma^2}}, \frac{\sigma_2}{L} \frac{C_{\Sigma^2}}{C_\Sigma}\right)} = \frac{\Gamma(\alpha, \beta_1)}{\Gamma(\alpha, \beta_2)} \\ f_r(r) &= \frac{\left(\beta_1/\beta_2\right)^\alpha}{B(\alpha, \alpha)} \frac{r^{\alpha-1}}{\left(r + \beta_1/\beta_2\right)^{2\alpha}} = \frac{\left(\sigma_1/\sigma_2\right)^\alpha}{B(\alpha, \alpha)} \frac{r^{\alpha-1}}{\left(r + \sigma_1/\sigma_2\right)^{2\alpha}} \end{aligned} \tag{H. 7}$$

which is the one of the classical RoA where change the shape parameter α. In the classical RoA we have $\alpha = NL$ whereas in the weighted RoA $\alpha = N_{eq}L$ with:

$$N_{eq} = \frac{C_{\Sigma}^2}{C_{\Sigma^2}} = \frac{\left(\sum_{i=1}^{N} c_i\right)^2}{\sum_{i=1}^{N} c_i^2} \tag{H. 8}$$

Now, presupposing a DxD filtering window with the smaller sub-window side length equal to M (in Section 3.3.1 we have referred to it with the letter *W*), the following relations hold:

$$\begin{aligned} M &= \frac{(D-1)}{2} \\ N &= MD \end{aligned} \tag{H. 9}$$

At this point, considering negative exponential weights going far from the central pixels but constant along the direction parallel to the orientation we have:

$$\begin{aligned} C_{\Sigma} &= \sum_{i=1}^{N} c_i = \sum_{i=0}^{M-1} De^{-\alpha i} = D\sum_{i=0}^{M-1} e^{-\alpha i} = D\frac{1-e^{-\alpha M}}{1-e^{-\alpha}} \\ C_{\Sigma^2} &= \sum_{i=1}^{N} c_i^2 = \sum_{i=0}^{M-1} De^{-2\alpha i} = D\sum_{i=0}^{M-1} e^{-2\alpha i} = D\frac{1-e^{-2\alpha M}}{1-e^{-2\alpha}} \end{aligned} \tag{H. 10}$$

so that the equivalent number of pixels become:

$$N_{eq} = \frac{C_{\Sigma}^2}{C_{\Sigma^2}} = \frac{\left(D\frac{1-e^{-\alpha M}}{1-e^{-\alpha}}\right)^2}{D\frac{1-e^{-2\alpha M}}{1-e^{-2\alpha}}} \tag{H. 11}$$

that is, studying the N_{Eq} asymptotic limits:

- $N_{Eq} \to D$ for $\alpha \to \infty$;
- $N_{Eq} \to N$ for $\alpha \to 0$.

The behavior of N_{Eq} varying *D* is shown in Fig. H.1 for the exponential coefficient $\alpha = 0.2$.

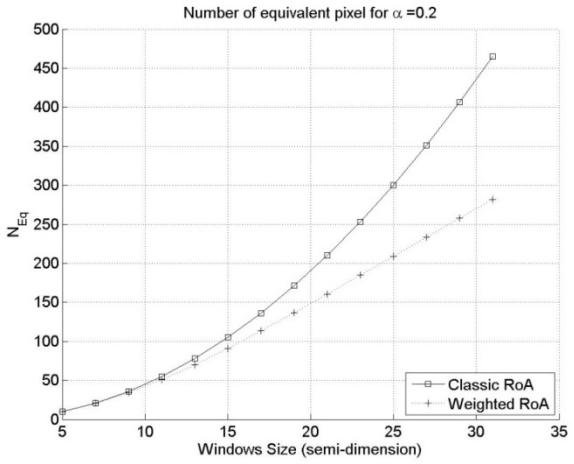

Fig. H.1 - N_{Eq} varying *D* with the weighted RoA with exponential coefficient $\alpha = 0.2$ superimposed to the classic RoA.

Appendix I

Filter Implementation

Several methods exists to implement discrete convolution (i.e. LTI filtering). Given a discrete signals $x[n]$ and a filter $h[n]$, respectively of length *X* and *H*, their convolution $y[n]$ is:

$$y[n] = x * h[n] = \sum_{p=-\infty}^{\infty} x[p]h[n-p] \tag{I.1}$$

with $y[n]$ of length $X + H - 1$. A direct computation of Eq. (I.1), when $H \leq X$, would require $(H+1)H + (X-H)H$ multiplications and addictions. An efficient method to compute direct convolution is to exploit Fast Fourier Transform properties and the circular convolution theorem.

In fact, considering $x[n]$ and $h[n]$ as periodic signal of equally length period *N* (i.e. padding with zero the smaller signal), the circular convolution theorem gives:

$$y[n] = x \otimes h[n] = \sum_{p=0}^{N-1} x[p]h[n-p] \xrightarrow{\text{DFT}_N} Y[k] = X[k]H[k] \tag{I.2}$$

where DFT_N indicates the N-points discrete FT (DFT):

$$Y[k] = \sum_{n=0}^{N-1} y[n] e^{-j2\pi \frac{k}{N} n} \tag{I.3}$$

Now, it is also well-known that given the aperiodic *N*-length version of signals $x[n]$ and $h[n]$, their linear convolution, which has length *2N-1*, can be computed by circular convolution with the previous signals zero-padded to have *2N-1* samples. Hence, exploiting FFT algorithms, linear convolution can be computed by *2N-1* points FFT of the signals, i.e. $X[k]$ and $H[k]$, successively multiplying the two transforms $Y[k] = X[k]H[k]$, and bringing $Y[k]$ in time with the *2N-1* points inverse FFT (IFFT):

$$y[n] = \frac{1}{2N-1} \sum_{n=0}^{2N-1} Y[k] e^{-j2\pi \frac{k}{2N-1} n} \tag{I.4}$$

Usually, the FFT of a signal of size *M* requires $CM \log_2 M$ operations, with *C* that depends on the FFT algorithm (e.g. the split-radix FFT has $C = 4$). Moreover, when the signal is real, exploiting hermitian symmetry ($X[-k] = X^*[k]$), *C* is halved by 2. Hence, in order to implement linear convolution of length *2N-1* by FFT, at least $3\frac{C}{2}(2N-1)\log_2(2N-1)$ operations are required (i.e. two *2N-1* points FFT and one *2N-1* points IFFT). Usually, when both $x[n]$ and $h[n]$ have small support, direct computation is faster, whereas the FFT method has less computational burden when signal supports raise.

Anyway, when the filter $h[n]$ has infinite support (IIR filter), direct computation can only be approximated truncating or multiplying with an appropriate window $w[n]$ the original filter $h[n]$.

Nevertheless, a very fast way to implement even this case exist when the Z-transform of $h[n]$ can be expressed in a rational form. In fact, in this last case a recursive implementation of the convolution $y[n] = x * h[n]$ is given by:

$$\sum_{i=0}^{N} a_i x[n-i] = \sum_{j=0}^{M} b_j y[n-j] \tag{I.5}$$

whose Z-transform can be expressed as:

$$H(z)=\frac{Y(z)}{X(z)}=\frac{\sum_{j=0}^{M} b_j z^{-j}}{\sum_{i=0}^{N} a_i z^{-i}} \tag{I.6}$$

If the denominator is not equal to 1 (i.e. $a_i \neq 0$ for some $i>0$) the recursive implementation could be applied and it requires only $N+M$ multiplications and addictions to obtain the final result.

In the following, a summary of edge detection filter coefficients, both in discrete-time and in Z-domain will be given. Filter functions and their Z-transformed version (when exists) will be summarized for discrete implementation purpose. Moreover, for recursive filtering, the Z-transform $H(Z)$ of the filter $h[n]$ will always be given as:

$$H(Z) = H_+(Z) + H_-(Z) \tag{I.7}$$

that is the sum of the causal component $H_+(Z)$ and the anticausal component $H_-(Z)$.

Canny filter 1-D

Canny filter in discrete-time is:

	Time-domain	**Constants**
Filter	$h[n]=-c\frac{n}{\sigma^2}e^{-\frac{n^2}{2\sigma^2}}$	$c=1\Big/\sum_{n=-\infty}^{\infty}\frac{\lvert n\rvert}{\sigma^2}e^{-\frac{n^2}{2\sigma^2}}$

The Z-transform of this function cannot be given in rational form and, consequently, fast recursive filtering cannot be implemented.

Deriche Filter 1-D

Deriche filter in discrete-time is:

	Time-domain	**Constants**
Filter	$h[n]=-ce^{-\alpha\lvert n\rvert}\sin(\omega_0 n)$ $=\begin{cases}-\frac{c}{2j}e^{(j\omega_0-\alpha)n}+\frac{c}{2j}e^{-(j\omega_0+\alpha)n}, & n\geq 0\\ -\frac{c}{2j}e^{(j\omega_0+\alpha)n}+\frac{c}{2j}e^{-(j\omega_0-\alpha)n}, & n<0\end{cases}$ $=\begin{cases}\alpha_1 p_1^n+\alpha_1^*\left(p_1^*\right)^n, & n\geq 0\\ \alpha_1 p_2^n+\alpha_1^*\left(p_2^*\right)^n, & n<0\end{cases}$	$\alpha_1=-\frac{c}{2j};$ $p_1=e^{-\alpha+j\omega_0};$ $p_2=e^{\alpha+j\omega_0};$

and in Z-domain:

	Z-domain	**Constants**
Filter	$H_+(z)=\frac{\alpha_1}{1-p_1 z^{-1}}+\frac{\alpha_1^*}{1-p_1^* z^{-1}}=\frac{a_1 z^{-1}}{1+b_1 z^{-1}+b_2 z^{-2}};$ $H_-(z)=\frac{\alpha_1 p_1^* z}{1-p_1^* z}+\frac{\alpha_1^* p_1 z}{1-p_1 z}=\frac{-a_1 z}{1+b_1 z+b_2 z}$	$a_1=-ce^{-\alpha}\sin(\omega_0);$ $b_1=-2e^{-\alpha}\cos(\omega_0);$ $b_2=e^{-2\alpha};$

To have unitary l_1-norm:

$$\sum_{n=-\infty}^{\infty}\lvert h[n]\rvert=1 \;\Rightarrow H_+(z)\big|_{z=1}=\frac{1}{2} \;\Rightarrow c=\frac{1-2e^{-\alpha}\cos(\omega_0)+e^{-2\alpha}}{2\left[e^{-\alpha}\sin(\omega_0)\right]} \tag{I.8}$$

Paillou Filter 1-D

Paillou filter in discrete-time is:

	Time-domain	Constants
Filter	$h[n]=-ce^{-\alpha\lceil n\rceil}\sinh(\omega_0 n)=$ $=\begin{cases}-\frac{c}{2}e^{(\omega_0-\alpha)n}+\frac{c}{2}e^{-(\omega_0+\alpha)n}, & n\geq 0\\ -\frac{c}{2}e^{(\omega_0+\alpha)n}+\frac{c}{2}e^{-(\omega_0-\alpha)n}, & n<0\end{cases}$ $=\begin{cases}\alpha_1\left(p_1p_2\right)^n-\alpha_1\left(p_1^{-1}p_2\right)^n, & n\geq 0\\ \alpha_1\left(p_1p_2^{-1}\right)^n-\alpha_1\left(p_1^{-1}p_2^{-1}\right)^n, & n<0\end{cases}$	$\alpha_1=-\frac{c}{2};$ $p_1=e^{\omega_0};$ $p_2=e^{-\alpha};$

and in Z-domain:

	Z-domain	Constants
Filter	$H_+(z)=\frac{a_1z^{-1}}{1+b_1z^{-1}+b_2z^{-2}};$ $H_-(z)=\frac{-a_1z}{1+b_1z+b_2z}$	$a_1=-ce^{-\alpha}\sinh(\omega_0);$ $b_1=-2e^{-\alpha}\cosh(\omega_0);$ $b_2=e^{-2\alpha}$

To have unitary l_1-norm:

$$\sum_{n=-\infty}^{\infty}|h[n]=1\ \Rightarrow H_+(z)\big|_{z=1}=\frac{1}{2}\ \Rightarrow c=\frac{1-2e^{-\alpha}\cosh(\omega_0)+e^{-2\alpha}}{2\left[e^{-\alpha}\sinh(\omega_0)\right]} \tag{I.9}$$

Shen-Castan Filter 1-D

Shen-Castan filter in discrete-time is:

	Time-domain	Constants
Filter	$h[n]=\begin{cases}-ce^{-\alpha n}, & n>0\\ 0, & n=0\\ ce^{\alpha n}, & n<0\end{cases}$	-

and in Z-domain:

	Z-domain	Constants
Filter	$H_+(z)=\frac{a_1z^{-1}}{1+b_1z^{-1}};$ $H_-(z)=\frac{-a_1z}{1+b_1z}$	$a_1=cb_1;$ $b_1=-e^{-\alpha}$

To have unitary l_1-norm:

$$\sum_{n=-\infty}^{\infty}|h[n]=1\ \Rightarrow H_+(z)\big|_{z=1}=\frac{1}{2}\ \Rightarrow c=\frac{1-e^{-\alpha}}{2e^{-\alpha}} \tag{I.10}$$

Canny Filter 2-D

Canny filter in discrete-time is:

	Time-domain	Constants
High-Pass	$h[n] = -c\frac{n}{\sigma^2}e^{-\frac{n^2}{2\sigma^2}}$	$c = 1 \Big/ \sum_{n=-\infty}^{\infty} \frac{\lvert n\rvert}{\sigma^2} e^{-\frac{n^2}{2\sigma^2}}$
Low-Pass	$h[n] = c_0 e^{-\frac{n^2}{2\sigma^2}}$	$c_0 = 1 \Big/ \sum_{n=-\infty}^{\infty} e^{-\frac{n^2}{2\sigma^2}}$

Deriche Filter 2-D

Deriche filter in discrete-time is:

	Time-domain	Constants
High-Pass	$h[n] = -ce^{-\alpha\lvert n\rvert}\sin(\omega_0 n)$	$c = \frac{1-2e^{-\alpha}\cos(\omega_0)+e^{-2\alpha}}{2[e^{-\alpha}\sin(\omega_0)]}$
Low-Pass	$h[n] = c_0 e^{-\alpha\lvert n\rvert}[\alpha\sin(\omega_0\lvert n\rvert)+\omega_0\cos(\omega_0\lvert n\rvert)]$	$c_0 = \frac{1-2e^{-\alpha}\cos(\omega_0)+e^{-2\alpha}}{2\alpha\sin(\omega_0)e^{-\alpha}+\omega_0-\omega_0 e^{-2\alpha}}$

and in Z-domain:

	Z-domain	Constants
High-Pass	$H(z) = \frac{a_1 z^{-1}}{1+b_1 z^{-1}+b_2 z^{-2}} - \frac{a_1 z}{1+b_1 z+b_2 z}$	$a_1 = -ce^{-\alpha}\sin(\omega_0)$ $b_1 = -2e^{-\alpha}\cos(\omega_0)$ $b_2 = e^{-2\alpha}$
Low-Pass	$H(z) = \frac{a_0+a_1 z^{-1}}{1+b_1 z^{-1}+b_2 z^{-2}} + \frac{a_2 z+a_3 z^2}{1+b_1 z+b_2 z}$	$c_1 = c_0\alpha$ $c_2 = c_0\omega_0$ $a_0 = c_2$ $a_1 = [c_1\sin(\omega_0)-c_2\cos(\omega_0)]e^{-\alpha}$ $a_2 = a_1 - c_2 b_1$ $a_3 = -c_2 b_2$ $b_1 = -2e^{-\alpha}\cos(\omega_0)$ $b_2 = e^{-2\alpha}$

Paillou Filter 2-D

Paillou filter in discrete-time is:

	Time-domain	Constants
High-Pass	$h[n] = -ce^{-\alpha\lvert n\rvert}\sinh(\omega_0 n)$	$c = \frac{1-2e^{-\alpha}\cosh(\omega_0)+e^{-2\alpha}}{2[e^{-\alpha}\sinh(\omega_0)]}$
Low-Pass	$h[n] = c_0 e^{-\alpha\lvert n\rvert}[\alpha\sinh(\omega_0\lvert n\rvert)+\omega_0\cosh(\omega_0\lvert n\rvert)]$	$c_0 = \frac{1-2e^{-\alpha}\cosh(\omega_0)+e^{-2\alpha}}{2\alpha\sinh(\omega_0)e^{-\alpha}+\omega_0-\omega_0 e^{-2\alpha}}$

and in Z-domain:

	Z-domain	Constants
High-Pass	$H(z)=\frac{a_1 z^{-1}}{1+b_1 z^{-1}+b_2 z^{-2}}-\frac{a_1 z}{1+b_1 z+b_2 z}$	$a_1=-ce^{-\alpha}\sinh(\omega_0)$ $b_1=-2e^{-\alpha}\cosh(\omega_0)$ $b_2=e^{-2\alpha}$
Low-Pass	$H(z)=\frac{a_0+a_1 z^{-1}}{1+b_1 z^{-1}+b_2 z^{-2}}+\frac{a_2 z+a_3 z^2}{1+b_1 z+b_2 z}$	$c_1=c_0\alpha$ $c_2=c_0\omega_0$ $a_0=c_2$ $a_1=[c_1\sinh(\omega_0)-c_2\cosh(\omega_0)]e^{-\alpha}$ $a_2=a_1-c_2\,b_1$ $a_3=-c_2\,b_2$ $b_1=-2e^{-\alpha}\cosh(\omega_0)$ $b_2=e^{-2\alpha}$

Shen-Casten 2-D

Shen Castan filter in discrete-time is:

	Time-domain	Constants
High-Pass	$h[n]=\begin{cases}-ce^{-\alpha n}, & n>0\\ 0, & n=0\\ ce^{\alpha n}, & n<0\end{cases}$	$c=\frac{1-e^{-\alpha}}{2e^{-\alpha}}$
Low-Pass	$h[n]=-c_0 e^{-\alpha\lvert n\rvert}$	$c_0=\frac{1-e^{-\alpha}}{1+e^{-\alpha}}$

and in Z-domain:

	Z-domain	Constants
High-Pass	$H(z)=\frac{a_1 z^{-1}}{1+b_1 z^{-1}}-\frac{a_1 z}{1+b_1 z}$	$a_1=cb_1$ $b_1=-e^{-\alpha}$
Low-Pass	$H(z)=\frac{a_0}{1+b_1 z^{-1}}+\frac{a_1 z}{1+b_1 z}$	$a_0=c_0$ $a_1=-c_0 b_1$ $b_1=-e^{-\alpha}$

Appendix J

SEL Path Metric

Given a pixel $(x,y)_n$ with an estimate path direction $\hat{\theta}_n$, the probability of a path crossing $(x,y)_n$ with a direction θ_n is indicated as $P(\theta_n|\hat{\theta}_n)$. Clearly, considering a first order Markov process:

$$P(\theta_n|\hat{\theta}_n,\cdots,\hat{\theta}_0) = P(\theta_n|\hat{\theta}_n) \tag{J. 1}$$

where θ_n and $\hat{\theta}_n$ are statistically independent from their respective previous steps:

$$\begin{aligned} P(\theta_n,\cdots,\theta_0) &= \prod_{i=0}^{n} P(\theta_i) \\ P(\hat{\theta}_n,\cdots,\hat{\theta}_0) &= \prod_{i=0}^{n} P(\hat{\theta}_i) \end{aligned} \tag{J. 2}$$

the metric $P(p)$ at step n becomes:

$$P(\theta_n,\cdots,\theta_0|\hat{\theta}_n,\cdots,\hat{\theta}_0) = P(\theta_n|\hat{\theta}_n,\cdots,\hat{\theta}_0)P(\theta_{n-1}|\hat{\theta}_{n-1},\cdots,\hat{\theta}_0)\cdots P(\theta_0|\hat{\theta}_0) \tag{J. 3}$$

so that, exploiting the previous hypothesis:

$$\begin{aligned} &P(\theta_n,\cdots,\theta_0|\hat{\theta}_n,\cdots,\hat{\theta}_0) = P(\theta_n|\hat{\theta}_n,\cdots,\hat{\theta}_0)P(\theta_{n-1}|\hat{\theta}_{n-1},\cdots,\hat{\theta}_0)\cdots P(\theta_0|\hat{\theta}_0) \\ &= P(\hat{\theta}_n,\cdots,\hat{\theta}_0|\theta_n)\frac{P(\theta_n)}{P(\hat{\theta}_n,\cdots,\hat{\theta}_0)}P(\hat{\theta}_{n-1},\cdots,\hat{\theta}_0|\theta_{n-1})\frac{P(\theta_{n-1})}{P(\hat{\theta}_{n-1},\cdots,\hat{\theta}_0)}\cdots P(\hat{\theta}_0|\theta_0)\frac{P(\theta_0)}{P(\hat{\theta}_0)} \\ &= \prod_{i=0}^{n} P(\hat{\theta}_i|\theta_i)\frac{P(\theta_n)}{\prod_{i=0}^{n}P(\hat{\theta}_i)}\prod_{i=0}^{n-1} P(\hat{\theta}_i|\theta_i)\frac{P(\theta_{n-1})}{\prod_{i=0}^{n-1}P(\hat{\theta}_i)}\cdots P(\hat{\theta}_0|\theta_0)\frac{P(\theta_0)}{P(\hat{\theta}_0)} \\ &= \frac{\prod_{i=0}^{n}P(\theta_i|\hat{\theta}_i)}{P(\theta_n)^{n-1}}\frac{\prod_{i=0}^{n-1}P(\theta_i|\hat{\theta}_i)}{P(\theta_n)^{n-2}}\cdots P(\theta_0|\hat{\theta}_0) \\ &= \frac{P(\theta_n|\hat{\theta}_n)}{P(\theta_n)^{n-1}}\frac{P(\theta_{n-1}|\hat{\theta}_{n-1})}{P(\theta_n)^{n-2}}\cdots P(\theta_0|\hat{\theta}_0) \end{aligned} \tag{J. 4}$$

that is:

$$P(\theta_n,\cdots,\theta_0|\hat{\theta}_n,\cdots,\hat{\theta}_0) \approx P(\theta_n|\hat{\theta}_n)P(\theta_{n-1}|\hat{\theta}_{n-1})\cdots P(\theta_0|\hat{\theta}_0) \tag{J. 5}$$

Appendix K

Improved Parametric (LR) Model

Indicating with $P(E_{\theta_k})$ (or $P(\overline{E}_{\theta_k})$) the probability to have (or not) an edge with direction θ_k at pixel *i*, and supposing the variables $r_i^{\theta_k}$ independent (previously indicated as r_{i,θ_k}), the improved GLR is:

$$\ln \lambda_i = \frac{P_{H_{E_{\theta_1}}}(r_i^{\theta_1}) P_{H_{E_{\theta_1}}}(r_i^{\theta_2}) P_{H_{E_{\theta_1}}}(r_i^{\theta_3}) P_{H_{E_{\theta_1}}}(r_i^{\theta_4})}{P_{H_{\overline{E}_{\theta_1}}}(r_i^{\theta_1}) P_{H_{\overline{E}_{\theta_1}}}(r_i^{\theta_2}) P_{H_{\overline{E}_{\theta_1}}}(r_i^{\theta_3}) P_{H_{\overline{E}_{\theta_1}}}(r_i^{\theta_4})} \tag{K. 1}$$

Following the passages in Section 3.3, presupposing the following statements true:

$$\begin{aligned} &\theta_1 \perp \theta_3 \\ &|\theta_1 - \theta_2| = |\theta_3 - \theta_4| = \pi/4 \end{aligned} \tag{K. 2}$$

we have:

$$\begin{aligned} P_{H_{\overline{E}_{\theta_1}}}(r_i^{\theta_3}) = [&P(E_{\theta_3}) P(r_i^{\theta_3} | E_{\theta_3}) + P(E_{\theta_2}) P(r_i^{\theta_3} | E_{\theta_2}) + \\ &+ P(E_{\theta_4}) P(r_i^{\theta_3} | E_{\theta_4}) + P(\overline{E}) P(r_i^{\theta_3} | \overline{E})] \end{aligned} \tag{K. 3}$$

Practically speaking, the pdf of the pixels of an image filtered with RoA using a filtering window with a direction (θ_3) orthogonal to θ_1 conditioned to not to have an edge with direction θ_1 can be computed as composition of other conditional probabilities that can be known. In this case, not to have an edge with direction θ_1 means that there could be an edge with direction θ_3, or θ_2, or θ_4, or eventually there could be no edge at all.

Considering the probabilities to have an edge in a certain direction uniform, i.e. $P(E_{\theta_i}) = P(\overline{E}) = 1/5$, ($P(\overline{E})$ the probability of not having any edge at pixel *i*) and knowing that:

$$P(r_i^{\theta_3} | E_{\theta_2}) = P(r_i^{\theta_3} | E_{\theta_4}) \tag{K. 4}$$

we have:

$$P_{H_{\overline{E}_{\theta_1}}}(r_i^{\theta_3}) = \frac{1}{5}\left[P(r_i^{\theta_3} | E_{\theta_3}) + 2P(r_i^{\theta_3} | E_{\theta_2}) + P(r_i^{\theta_3} | \overline{E})\right] \tag{K. 5}$$

Now, since the conditional probabilities do not change, if we change the reference angle, we can indicate these probabilities taking as reference the variable under condition.

For example, if the direction θ_1 is taken as reference, we can write:

$$\begin{aligned} &\theta_1 = \theta_{//} \\ &\theta_3 = \theta_{\perp} \\ &\theta_2 = \theta_{\angle}^{A} \\ &\theta_4 = \theta_{\angle}^{B} \end{aligned} \tag{K. 6}$$

as consequence Eq. (K. 5) becomes:

$$P_{H_{\overline{E}_{\theta_1}}}(r_i^{\theta_3}) = \frac{1}{5}\left[P(r_i | E_{\theta_{\parallel}}) + 2P(r_i | E_{\theta_{\angle}}) + P(r_i | \overline{E})\right]_{r_i = r_i^{\theta_3}} \tag{K. 7}$$

Following the same previous reasoning for $P_{H_{\overline{E}_{\theta_1}}}\left(r_i^{\theta_1}\right)$, $P_{H_{\overline{E}_{\theta_1}}}\left(r_i^{\theta_2}\right)$ and $P_{H_{\overline{E}_{\theta_1}}}\left(r_i^{\theta_4}\right)$, knowing that $P_{H_{\overline{E}_{\theta_1}}}\left(r_i^{\theta_2}\right)=P_{H_{\overline{E}_{\theta_1}}}\left(r_i^{\theta_4}\right)$:

$$P_{H_{\overline{E}_{\theta_1}}}\left(r_i^{\theta_1}\right)=\frac{1}{5}\left[P\left(r_i\left|E_{\theta_\perp}\right.\right)+2P\left(r_i\left|E_{\theta_\angle}\right.\right)+P\left(r_i\left|\overline{E}\right.\right)\right]_{r_i=r_i^{\theta_1}} \tag{K. 8}$$

and

$$P_{H_{\overline{E}_{\theta_1}}}\left(r_i^{\theta_2}\right)=\frac{1}{5}\left[P\left(r_i\left|E_{\theta_{//}}\right.\right)+P\left(r_i\left|E_{\theta_\perp}\right.\right)+P\left(r_i\left|E_{\theta_\angle}\right.\right)+P\left(r_i\left|\overline{E}\right.\right)\right]_{r_i=r_i^{\theta_2}} \tag{K. 9}$$

Eventually, the general GLR can be written as:

$$\begin{aligned}
&\ln\lambda_i = 5^4\, P\left(r_i\left|E_{\theta_{//}}\right.\right)_{r_i=r_i^{\theta_1}} P\left(r_i\left|E_{\theta_\angle}\right.\right)_{r_i=r_i^{\theta_2}} P\left(r_i\left|E_{\theta_\angle}\right.\right)_{r_i=r_i^{\theta_4}} P\left(r_i\left|E_{\theta_\perp}\right.\right)_{r_i=r_i^{\theta_3}} \cdot \\
&\cdot\left\{\left[P\left(r_i\left|E_{\theta_\perp}\right.\right)+2P\left(r_i\left|E_{\theta_\angle}\right.\right)+P\left(r_i\left|\overline{E}\right.\right)\right]_{r_i=r_i^{\theta_1}}\right\}^{-1}\cdot \\
&\cdot\left\{\left[P\left(r_i\left|E_{\theta_{//}}\right.\right)+P\left(r_i\left|E_{\theta_\perp}\right.\right)+P\left(r_i\left|E_{\theta_\angle}\right.\right)+P\left(r_i\left|\overline{E}\right.\right)\right]_{r_i=r_i^{\theta_2}}\right\}^{-1}\cdot \\
&\cdot\left\{\left[P\left(r_i\left|E_{\theta_{//}}\right.\right)+P\left(r_i\left|E_{\theta_\perp}\right.\right)+P\left(r_i\left|E_{\theta_\angle}\right.\right)+P\left(r_i\left|\overline{E}\right.\right)\right]_{r_i=r_i^{\theta_4}}\right\}^{-1} \\
&\cdot\left\{\left[P\left(r_i\left|E_{\theta_{//}}\right.\right)+2P\left(r_i\left|E_{\theta_\angle}\right.\right)+P\left(r_i\left|\overline{E}\right.\right)\right]_{r_i=r_i^{\theta_3}}\right\}^{-1}
\end{aligned}$$

Now, considering the following pdf:

$$f_r(r)=\frac{\Gamma(\alpha_1+\alpha_2)}{\Gamma(\alpha_1)\Gamma(\alpha_2)}\left[\left(\frac{\beta_1}{\beta_2}\right)^{\alpha_2}\frac{r^{\alpha_1-1}}{\left(r+\frac{\beta_1}{\beta_2}\right)^{\alpha_1+\alpha_2}}+\left(\frac{\beta_2}{\beta_1}\right)^{\alpha_1}\frac{r^{\alpha_2-1}}{\left(r+\frac{\beta_2}{\beta_1}\right)^{\alpha_1+\alpha_2}}\right] \tag{K. 10}$$

all the previous pdfs are equal to $f_r(r)$ in Eq. (K. 10) with certain values of α and β. In the general case these values are:

$$\begin{aligned}
\alpha_1&=\frac{L(S_1\sigma_1+S_2\sigma_2)^2}{S_1{\sigma_1}^2+S_2{\sigma_2}^2} \qquad \beta_1=\frac{S_1{\sigma_1}^2+S_2{\sigma_2}^2}{NL(S_1\sigma_1+S_2\sigma_2)} \\
\alpha_2&=\frac{L(D_1\sigma_1+D_2\sigma_2)^2}{D_1{\sigma_1}^2+D_2{\sigma_2}^2} \qquad \beta_2=\frac{D_1{\sigma_1}^2+D_2{\sigma_2}^2}{NL(D_1\sigma_1+D_2\sigma_2)}
\end{aligned} \tag{K. 11}$$

Then, indicating with w the dimension of the filtering window (e.g. a window 11x11 has *w=11*) and with $m=\lfloor(w-1)/2\rfloor$ the truncated round (e.g. for the previous example *m=5*):

$$P\left(r_i\left|E_{\theta_\perp}\right.\right)\rightarrow\begin{cases}S_1=(m+1)m\\S_2=N-S_1\\D_1=S_1\\D_2=S_2\end{cases} \tag{K. 12}$$

$$P\left(r_i \left| E_{\theta_{//}} \right.\right) \rightarrow \begin{cases} S_1 = wm \\ S_2 = 0 \\ D_1 = S_1 \\ D_2 = S_2 \end{cases} \tag{K. 13}$$

$$P\left(r_i \left| E_{\theta_{\angle}} \right.\right) \rightarrow \begin{cases} S_1 = \sum_{i=1}^{m} i \\ S_2 = N - S_1 \\ D_1 = \sum_{i=m+2}^{w} i = 3S_1 \\ D_2 = N - D_1 = S_2 - 2S_1 \end{cases} \tag{K. 14}$$

Appendix L

Measure of Backscattering Coefficients at Different Incidence Angles

When surfaces are not flat (and not unbounded as well), the Snell's law which rules the reflection and refraction of an incident electromagnetic (EM) wave on an interface between two media is no longer valid. Usually, on real surfaces, two backscattering contributes are separated: a coherent contributes which is due to the specular reflection of the incidence EM wave and an incoherent contribute due to the surface roughness. The surface roughness is generally described statistically by the standard deviation σ_h of the surface height. In fact, locally, if an ideal monochrome EM wave hits a surface of a certain height h, it will be subjected to a phase shift $\Delta\phi$ proportional to h and to the incidence angle θ between the wave and the normal of the surface. Following the Rayleigh criterion, a surface is said to be rough if $\Delta\phi > \pi/2$ i.e.:

$$\sigma_h > \lambda/8\cos\theta \tag{L. 1}$$

where λ is the wave length of EM wave. From Eq. (L. 1) is clear that the higher the roughness, the more the backscattering diagram differs from that of a flat interface. Moreover, it depends on the angle of incidence, in particular, the wider the angle of incidence, the more significant the roughness, and the more perturbed the radiation diagram.

Hence, on SAR images a contrast improvement between grass field and runway asphalt can be obtained exploiting this relation. Usually, the reflection characteristic of a certain material is related to the transmitting EM wave in term of backscattering coefficients. The EM field in the plane orthogonal to the EM wave propagation direction can be divided in a sum of two orthogonal components, called polarizations, respectively indicated as H (horizontal) and V (vertical). Then, given the linear behaviour of the reflection system, even the received EM field can be divided in the same manner, and the relation between the two fields is given by the backscattering matrix:

$$S = \begin{bmatrix} S_{HH} & S_{HV} \\ S_{VH} & S_{VV} \end{bmatrix} \tag{L. 2}$$

which is symmetric for the reciprocity principle. Anyway, transmitting and receiving with the same polarization, only S_{HH} or S_{VV} have to be studied.

In order to quantitatively measure the dependence between incidence angle and received RCS an analysis of backscattering coefficients[16] for X band transmission has been carried on. As can be seen in Fig. L.1 both S_{HH} and S_{VV} go down when θ raises. Anyway, in Fig. L.2 where the logarithm of the ratio of S_{HH} (and S_{VV}) between two type of material is plot for different θ we can see that polarization HH enables us to decrease more the ratio when θ raises, i.e. to enhance more the RCS contrast. Finally, in Fig. L.3 a cue to what previously maintained is reported. As we can see the incidence angle strongly enhance the contrast between different materials exploiting the roughness difference.

[16] Stored in a database which is property of IDS - Ingegneria Dei Sistemi Company.

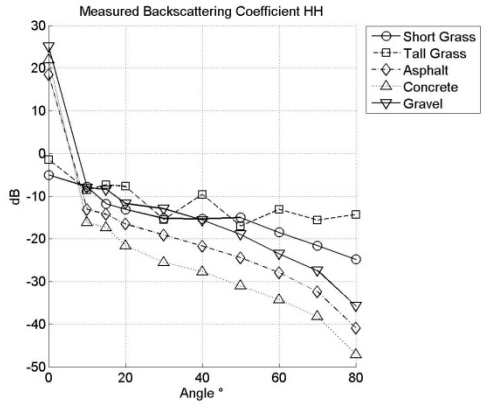

(a)

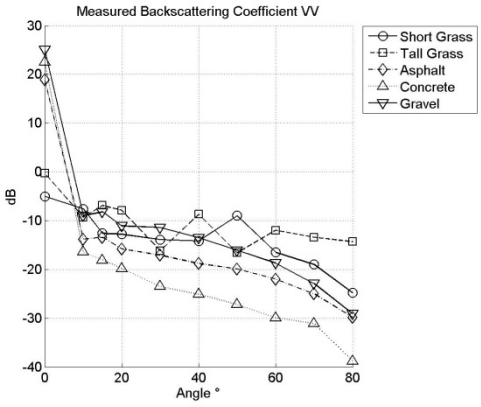

(b)

Fig. L.1 - (a) Logarithm of S_{HH} coefficient varying the incidence angle for different type of material. (b) Logarithm of S_{VV} coefficient varying the incidence angle for different type of material

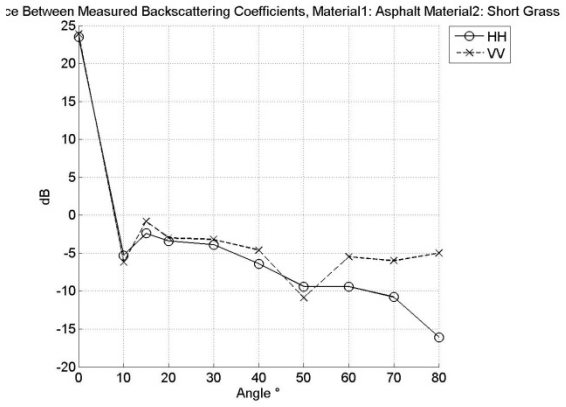

Asphalt - Short Grass

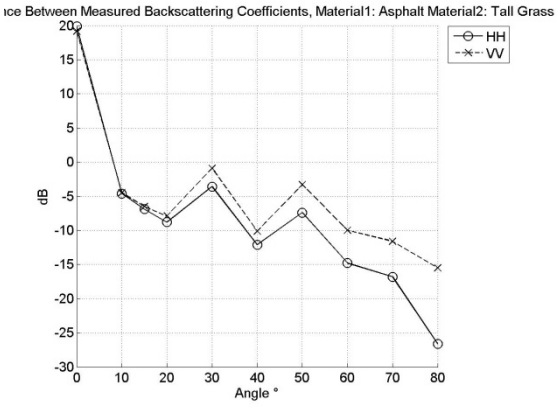

Asphalt - Tall Grass

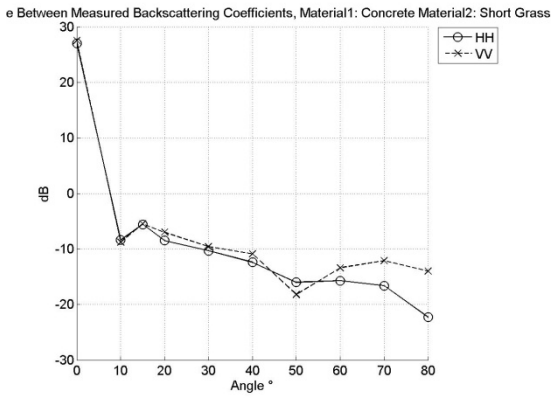

Concrete - Short Grass

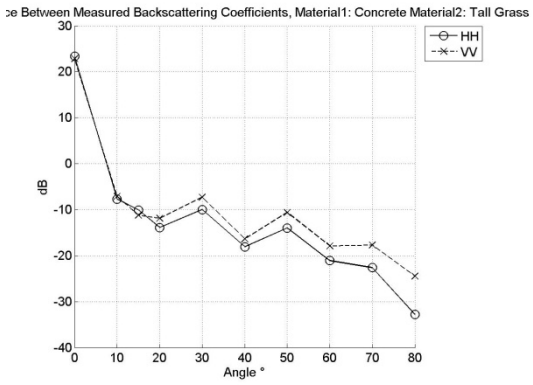

Concrete - Tall Grass

Fig. L.2 - Difference between the S_{HH} (and S_{VV}) logarithm for two different materials (i.e. the logarithm of the ratio) varying the incidence angle.

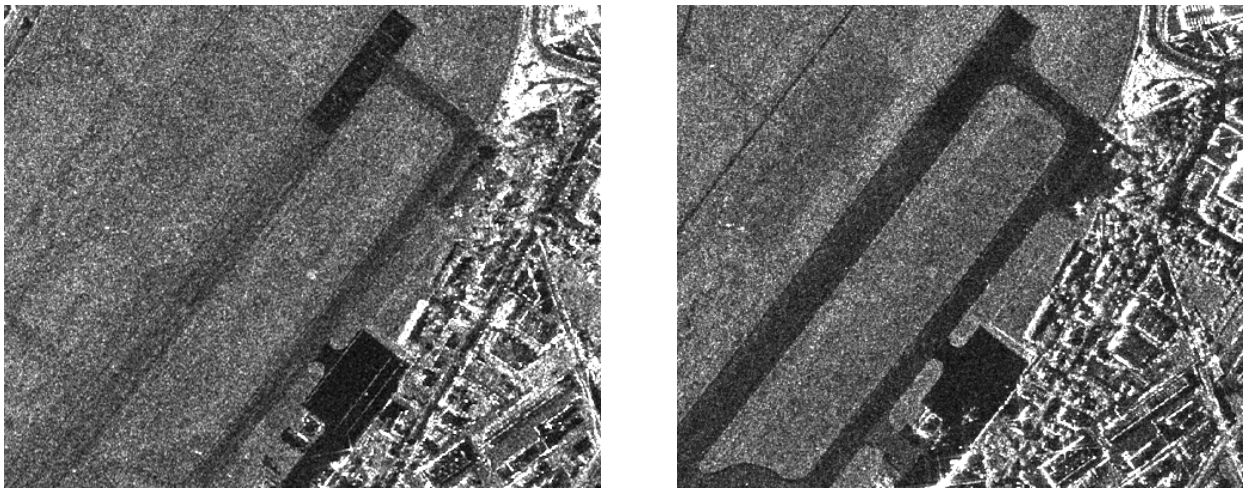

(a) (b)

Fig. L.3 - (a) Amplitude CSK image with incidence angle near/far 26.5°/27.4°. (b) Amplitude CSK image with incidence angle near/far 55.9°/56.3°

Appendix M

PDE Filters Implementation

PDE based filters are very sensitive to numeric implementation used [73]. Usually, implementation of derivative operators is performed by using finite differences as:

$$\begin{aligned}
\frac{dI}{dx} &\approx \frac{I\left(x+\frac{\Delta x}{2},y\right)-I\left(x-\frac{\Delta x}{2},y\right)}{\Delta x};\\
\frac{dI}{dy} &\approx \frac{I\left(x,y+\frac{\Delta y}{2}\right)-I\left(x,y-\frac{\Delta y}{2}\right)}{\Delta y};\\
\frac{dI}{dt} &\approx \frac{I^{t+1}-I^{t}}{\Delta t};
\end{aligned} \tag{M. 1}$$

whereas the iterative approximation of the continuous PDE may essentially be done by two type of approach, namely explicit and implicit.

Explicit approaches are the straightforward discretization of the continuous PDE equation, which in 1-D is:

$$\begin{aligned}
I_t &= \frac{d}{dx}\left[g(x)I_x\right]\\
\frac{I^{t+1}-I^{t}}{\Delta t} &= \frac{d}{dx}\left[g(x)\frac{I(x+\Delta x/2)-I(x-\Delta x/2)}{\Delta x}\right]\\
\frac{I^{t+1}-I^{t}}{\Delta t} &= \frac{1}{\Delta x}\left[g(x+\Delta x/2)\frac{I(x+\Delta x)-I(x)}{\Delta x}-g(x-\Delta x/2)\frac{I(x)-I(x-\Delta x)}{\Delta x}\right]\\
\frac{I^{t+1}-I^{t}}{\Delta t} &= \frac{1}{\Delta x^{2}}\left\{g(x+\Delta x/2)\left[I(x+\Delta x)-I(x)\right]+g(x-\Delta x/2)\left[I(x-\Delta x)-I(x)\right]\right\}\\
I^{t+1} &= \frac{\Delta t}{\Delta x^{2}}\left(J_R+J_L\right)+I^{t}
\end{aligned} \tag{M. 2}$$

where J_R and J_L are respectively the flux on the right and on the left at position *x*. Clearly, Eq. (M. 2) can be written in a matrix notation as:

$$I^{t+1}=\left(I_d+\Delta tA\right)I^{t} \tag{M. 3}$$

where I_d is the identity matrix.

Instead, implicit approaches need a matrix inversion (i.e. solving a linear system) at each step, because are of the type:

$$\begin{aligned}
\frac{I^{t+1}-I^{t}}{\Delta t} &= AI^{t+1}\\
I^{t+1} &= \left(I_d-\Delta tA\right)^{-1}I^{t}
\end{aligned} \tag{M. 4}$$

With the former approaches (explicit schemas), the time step Δt has to respect a tight constraint (small time step) to avoid singularity generations with the benefit of a straightforward implementation. Instead, implicit schemas are more computational expensive and more complex to implement although they enable to use a greater time step (i.e. less number of iterations to reach the solution at the same time *t*). In [84] these aspects are treated in deep with the prospective of creating numerical schemas that preserve the same properties of the original PDE. Among these properties, the most important ones are: invariance to grey level shift, invariance to reverse contrast, invariance to image translation and rotation, average grey level preservation, and respect of the maximum-minimum principle. Maybe this last properties is the most fundamental one, i.e. the

grey levels of the final result are always inside the grey level interval of the initial image, that is, the initial image dynamic is not extended (it can only be reduced). In [84] is proved that explicit schemas which use finite differences (also called central differences) to approximate derivatives preserve the previous properties and the obtained numerical solution approximates the real solution with a very small error (relative Euclidean distance of 0.14%). Moreover, a simply implicit schema is proposed. It is based to an algorithm, namely the Thomas algorithm, which solve linear system which have tridiagonal matrixes and, for dimension bigger than 1 (as in the case of images), on the additive operator splitting (AOS) schema. This last operator is obtained separating the diffusion process in each orthogonal direction and summing each partial result at the end. This implicit schema has been proved to be absolutely stable for each time step Δt and this open a great question: Is it possible to obtain the final result with only one step of the algorithm? At this question is answered in [84] again, where is pointed out that increasing Δt too much yields big error in the final solution (relative Euclidean distance can reach 5%). Anyway, if we admit errors of about 2% in the relative Euclidean distance, the computational burden of AOS is ten times lesser than that of the explicit schema. Hence, in conclusion, choosing an implementation schema is equal to choosing a trade-off between accuracy and computational burden.

In order to have a fairly comparison among different PDE based filters with the greatest accuracy, an explicit implementation schema has been used for all filters.

All PDE filters use the simply finite difference to compute the gradient and at each step only a 4-connected neighbourhood of each pixel is involved to update its value.

Perona-Malik (PM) and SRAD filters use a homogeneous region passed as input to compute some parameters. In PM the parameter C_m and the threshold *k* are automatically computed. Parameter C_m is determined as zero of the equation:

$$\begin{gathered} \frac{d}{dx}\left[xg_1(x)\right]\Big|_{k=|\nabla I|} = 0 \\ \Downarrow \\ 1-(1+mC_m)e^{-C_m} = 0 \end{gathered} \tag{M. 5}$$

using Matlab function *fzero*.

Instead, the threshold *k* is computed as the quantile *Q* of the experimental cumulative density function (ecdf) of the respective variables to which the threshold has to be applied. In order to take advantage from the iterative quality improvement achieved by the filters, the quantile *Q* is computed each time through values of a homogeneous region provided in input.

Moreover, the iterations are stop when a step does not produce a relative difference bigger than 1.5e-3 on the coefficient of variation of the homogeneous region. Also SRAD share this stop condition, whereas CED makes 150 iterations with a time step of $\Delta t = 0.25$. This different stop condition of CED is needed because CED does not manages to smooth homogeneous regions as PM and SRAD.

An important improvement introduced in PM, CED and IEED filter implementation is the optimized gradient operator [84]. As previously said, finite differences were used for derivatives computation. Instead, as suggested in [84] the optimum 3x3 operator to obtain rotation invariance and minimum angular error is:

$$F_x = \frac{1}{32}\begin{bmatrix} -3 & 0 & 3 \\ -10 & 0 & 10 \\ -3 & 0 & 3 \end{bmatrix}; \qquad F_y = \frac{1}{32}\begin{bmatrix} -3 & -10 & -3 \\ 0 & 0 & 0 \\ 3 & 10 & 3 \end{bmatrix} \tag{M. 6}$$

This simple stencil manages to approximate rotation invariance significantly better than related popular stencils like the Sobel filters and moreover its Fourier Transform presents less Gibbs effect respect to the simple finite difference [84]. From a point of view different from rotation invariance optimization, it is well-known that a bigger derivative window is surely less sensitive to noisy data and gets an improved derivative estimation. Anyway, increasing the window size may get to a loss of fine gradient variations and a bias in the final computation. For this reason authors in [84] have chosen 3x3 windows as the right trade-off for anisotropic diffusion schemas. Moreover, the explicit numerical schema proposed in [84] combines the advantages of

classical (Euler-forward) explicit schemas of yielding a small error in final solution computation, with a higher efficiency (up to 4 times) typical of implicit or semi-implicit techniques. Indeed, a time step up to $\Delta t = 1$ can be used without compromising the numerical stability. Finally, the numerical computation in [84] can be directly implemented by simple convolution operations.

It should be noted that all these filters takes as input the logarithm of the Gaussian smoothed image I_{σ_1}, with $\sigma_1 = 2$. Anyway, before computing the gradient to use inside the diffusivity function an additional Gaussian smoothing with $\sigma_2 = 1$ is applied at each step as regularization. This last smoothing also manages to remove some spurious blobs that get rise on homogeneous regions when the gradient is badly estimated.

Appendix N

Despeckling Filters Parameters

Filter	Image	Window Size	PFA/ ENL (threshold)	Edge Detector
Lee	intensity	11x11	10^{-4}/ 1	RoA
Kuan	=	=	=	=
Frost ($\lambda = 0.2$)	=	=	=	=
Gamma	=	=	=	=
Mean	=	=	=	=

Tab. N.1 - Classic filter parameters

Filter	Image	Pre-smoothing	Regularization-smoothing	Time-step Normal/Rotat.Inv. (Implementation)	Stop criterion	Others
PM	log-intensity	$\sigma = 2$	$\sigma = 1$	0.25 / 1	Coefficient of variation	$m = 16$; $Q = 0.9$;
SRAD	=	=	$\sigma = 0.5$	0.25 / -	=	-
CED	=	=	$\sigma = 1$; $\rho = 4$	0.25 / 1	150 steps	$m = 2$; $\alpha = 0.05$;
IEED	=	=	$\sigma = 1$; $\rho = 2$	0.25 / 1	=	$m = 16$; $Q_1 = 0.9$; $Q_2 = 0.999$;

Tab. N.2 - PDE filter parameters

Filter	Image	ENL	W. Search/ W. Similarity	Q/ T	Iterations
PPB1	Amplitude	1	21/ 7	0.88/ Inf	1
PPB10	=	=	[3 7 11 21]/ [1 3 5 7]	0.92/ 0.2	[1 2 3 4]

Tab. N.3 - PPBi filter parameters

Filter	Image	ENL/ K	W. Estimation	Over-smoothing Factor
UWD	Amplitude	1/ 5	[11 13 15 17 19]	1

Tab. N.4 - UWD filter parameters

Bibliography

[1] D. Massonnet and J.-C. Souyris, *Imaging with Synthetic Aperture Radar*, EFPL Press, 2008.

[2] H. Maitre, *Processing of Synthetic Aperture Radar Images*, John Wiley & Sons, 2008.

[3] C. Oliver and S. Quegan, *Understanding Synthetic Aperture Radar Images*, Cap. 4, SciTech Publishing Inc., Raleigh (NC), 2004.

[4] H. Xie, L. E. Pierce, and F. T. Ulaby, "Statistical Properties of Logarithmically Transformed Speckle", *IEEE Transactions on Geoscience and Remote Sensing*, Vol.40, No.3, pp.712-727, March 2002.

[5] Redding N.J., "Estimating the Parameters of the K Distribution in the Intensity Domain", *Technical report DSTO−TR−0839*, DSTO Electronics and Surveillance Research Laboratory, Salisbury (Australia), 1999.

[6] F.T. Ulaby, F Kouyate,B. Brisco, and T.H L. Williams, "Textural Information in SAR Images", *IEEE Transactions on Geoscience and Remote Sensing*, vol.24, no.2, pp.235-245, March 1986.

[7] C. J. Oliver, "Optimum edge detection in SAR", *IEEE Proc. Radar, Sonar Navig.*, Vol. 143, No. 1, pp. 31-40, February 1996.

[8] R. Touzi, A. Lopes, and P. Bousquet, "A Statistical and Geometrical Edge Detector for SAR Images", *IEEE Transactions on Geoscience and Remote Sensing*, Vol. 26, No. 6, pp. 764-773, November 1988.

[9] M. Bauchemin, P. Keith, B. Thomson, and G. Edwards, "On Nonparametric Edge Detection in Multilook SAR Images", *IEEE Transactions on Geoscience and Remote Sensing*, Vol. 36, No. 5, pp. 1826-1829, September 1998.

[10] M. Abramowitz and I. A. Stegun, *Handbook of Mathematical Functions*., New York: Dover, 1965.

[11] Y. Cui, G. Zhou, J. Yang, and Y. Yamaguchi: "Unsupervised Estimation of the Equivalent Number of Looks in SAR Images" *IEEE Transactions on Geoscience and Remote Sensing*, Vol.8, No.4, pp.710-714, July 2011.

[12] B. L. Welch, "The significance of the difference between two means when the population variances are unequal", *Biometrika*, Vol. 29, No. 3/4, February 1938, pp. 350-362.

[13] A. C. Bovik, T. S. Huang, and D. C. Munson, Jr., "Nonparametric tests for edge detection in noise", *Pattern Recognit.*, Vol. 19, pp. 209–219, 1986.

[14] United States Air Force, Sensor Data Management System, Web, 10 September 2010, <https://www.sdms.afrl.af.mil/>.

[15] M. S. Greco and F. Gini: "Statistical Analysis of High-Resolution SAR Ground Clutter Data", *IEEE Transactions on Geoscience and Remote Sensing*, Vol.45, No.3, pp.566-575, March 2007.

[16] J. D. Echard: "Estimation of radar detection and false alarm probability," *IEEE Transactions on Aerospace and Electronic Systems*, Vol.27, No.2, pp.255-260, Mar 19901.

[17] Trevor Stewart, Leo Strijbosch, Hans Moors, Paul van Batenburg, "A Simple Approximation to the Convolution of Gamma Distributions", *CentER Discussion Paper*, No. 2006-27, April 2006.

[18] J. Shen, S. Castan, "An optimal linear operator for step edge detection", *Graphical Models and Image Processing*, Vol. 54, 112–133, 1992.

[19] V. S. Frost, J. A. Stiles, K. S. Shanmugan, J. C. Holtzman, "A Model for Radar Images and its Application to Adaptive Digital Filtering of Multiplicative Noise", *IEEE Transactions Pattern Analysis and Machine Intelligence*, Vol. PMI-6, No. 5, pp. 658-661, September 1984.

[20] J. W. Woods and J. Biemond, "Comments on 'A Model for Radar Images and its Application to Adaptive Digital Filtering of Multiplicative Noise' ", *IEEE Transactions Pattern Analysis and Machine Intelligence*, Vol. PMI-6, No. 5, pp. 658-661, September 1984.

[21] R. Fjørtoft, A. Lopes, P. Marthon, E. Cubero-Castan, "An Optimal Multiedge Detector for SAR Image Segmentation", *IEEE Transactions on Geoscience and Remote Sensing*, Vol. 36, No. 3, pp. 793-802, May 1998.

[22] R. Fjørtoft, P. Marthon and Armand Lopès: “Multiresolution Edge Detection in SAR Images”, 1997, [Online].

[23] N. Otsu, “A Tlreshold Selection Method from Gray-Level Histograms”, *IEEE Transactions On Systrems*, Man, And Cybernetics, Vol. Smc-9, No. 1, January 1979.

[24] A. K. C. Wong, and P. K. Sahoo, “A Gray-Level Threshold Selection Method Based on Maximum Entropy Principle”, *IEEE Transactions On Systems, Man. And Cybernetics*. Vol. 19, No. 4., 1989.

[25] Canny, J., “A Computational Approach To Edge Detection”, *IEEE Trans. Pattern Analysis and Machine Intelligence*. Vol. 8, No. 6, pp. 679-698, 1986.

[26] S. Mallat, *A Wavelet Tour of Signal Processing*, Academic Press, 1999.

[27] S. Mallat, and W.L. Hwang, “Singularity detection and processing with wavelets”. *IEEE Trans. Information Theory*, Vol. 38, No. 2, pp. 617–643, 1992.

[28] S. Mallat, and S. Zhong,”Characterization of signals from multiscale edges, *IEEE Transactions on Pattern Analysis and Machine Intelligence*, Vol. 14, No. 7, pp 710 – 732,1992.

[29] B. M. Sadler, and A. Swami, “Analysis of multiscale products for step detection and estimation”, *IEEE Trans. Information Theory*, Vol. 45, No. 3, pp. 1043–1051, 1999.

[30] M. Chabert, and J. Y. Tourneret, “Time-scale analysis of abrupt changes corrupted by multiplicative noise”, *Elsevier Signal Process*., Vol. 80, No. 3, pp. 397-411, 2000.

[31] L. Zhang , and P. Bao, “Edge detection by scale multiplication in wavelet domain”, *Pattern Recognition Letters*, Vol. 23, pp. 1771–1784, 2002.

[32] I. Daubechies, *Ten Lectures on Wavelets*, SIAM, Philadelphia, Pa, USA, 1992.

[33] J. Shen, S. Castan, “An optimal linear operator for step edge detection”, *Graphical Models and Image Processing*, Vol. 54, 112–133, 1992.

[34] R. Deriche, “Fast Algorithms for low level vision”, *IEEE Transactions On Pattern Analysis and Machine Intelligence*, Vol. 12, No. 1, January 1990.

[35] R. Deriche, “Using Canny's Criteria to Derive a Recursively Implemented Optimal Edge Detector”, *International Journal of Computer Vision*, pp. 167-187, 1987.

[36] P. Paillou, “Detecting Step Edges in Noisy SAR Images: A New Linear Operator”, *IEEE Trans. On Geoscience And Remote Sensing*, Vol. 35, No. 1, January 1997.

[37] W. K. Pratt, *Digital Image Processing*. New York: Wiley, 1978.

[38] R. C. Gonzalez and R. E. Woods, *Digital Image Processing*, Pearson Education Inc., Upper Saddle River New Jersey, 2008.

[39] A. C. Bovik, “On Detecting Edges in Speckle Imagery”, *IEEE Trans. Acoustics Speech and Signal Processing*, Vol. 36, No. 10, pp. 1618-1627, 1988.

[40] A. Martelli, “An application of heuristic search methods to edge and contour detection”, *Magazine Communications of the ACM*, Vol. 19, No. 2, February 1976.

[41] P. H. Eichel, E. J. Delp, K. Koral, and A. J. Buda, “A method for fully automatic definition of coronary arterial edges from cineangiograms,” *IEEE Trans. Med. Imaging*, Vol. 7, No. 4, pp. 313–320, 1988.

[42] A. A. Farag, and J. E. Delp, “Edge Linking By Sequential Search,” *Pattern Recognition*, Vol. 28, No. 5, pp. 611-633, 1995.

[43] G. W. Cook, and J. E. Delp; "Multiresolution sequential edge linking," *International Conference on Image Processing*, Vol. 1, pp. 41-44, 1995.

[44] G. W. Cook, and J. E. Delp, “Gaussian mixture model for edge-enhanced images,” *Journal of Electronic Imaging*, Vol. 13, No. 4, pp. 731-737, 2004.

[45] S. P. Meyn and R. L. Tweedie, *Markov Chains and Stochastic Stability*, Springer-Verlag, London, 1993.

[46] M. Kass, A. Witkin, and D. Terzopoulos, “Snakes: Active Contour Model”, *International Journal of Computer Vision*, Vol. 1, No. 4, pp. 321-331, 1988.

[47] X. Bresson, “Image Segmentation with Variational Active Contours”, Master Ph.D. Thesis, Paris, France, 2005.

[48] M. Jacob, T. Blu, and M. Unser, “Efficient Energies and Algorithms for Parametric Snakes”, *IEEE Transactions On Image Processing*, Vol. 13, No. 9, September 2004.

[49] P. E. Hart, N. J. Nilsson, and B. Raphael, “A Formal Basis for the Heuristic Determination of Minimum Cost Paths”, *IEEE Transactions Of Systems Science and Cybernetics*, Vol. 4, No. 2, July 1968.

[50] R. Bellman, "On A Routing Problem," *Quart. Appl. Math.*,No. 16, pp. 87-90, 1958.

[51] T. H. Cormen, C. E. Leiserson, R. L. Rivest, *Introduction to Algorithms*, MIT Press and McGraw-Hill, Second Edition, 2001.

[52] R. O. Duda and P. E. Hart, “Use of the Hough Transform to detect lines and curves in pictures”, *Communs Ass. comput. Mach.*, Vol. 15, pp. 11-15, 1975.

[53] K. V. Hansen and P. A. Toft, “Fast Curve Estimation Using Pre-Conditioned Generalized Radon Transform”, *IEEE Trans. Image Processing*, Vol. 5, pp. 1-651, 1996.

[54] S. R. Deans., *The Radon Transform and Some of Its Applications*, Krieger Publishing Company, Malabar Florida, (1993).

[55] W. C. Y. Lam, L. T. S. Lam, K. S. Y. Yuen, and D. N. K. Leung, “An analysis on quantizing the Hough space”, *Pattern Recognition Letters*, Vol. 15, pp. 1127-1135, November 1994.

[56] P. A. Rattey and A. G. Lindgren, “Sampling the 2-D Radon Transform”, *IEEE Trans. on Acoustic, Speech, and Signal Processing*, Vol. 29, No. 5, pp. 994-1002, October 1981.

[57] G. Papari and N. Pektov, “Edge and line oriented contour detection: State of the art”, *Image and Vision Computing*, Vol. 29, No. 2-3, pp. 79-103, 2011.

[58] D. T. Kuan, A. A. Sawchuk, T. C. Strand, and P. Chavel, “Adaptive noise smoothing filter for images with signal-dependent noise,” *IEEE Trans. Pattern Anal. Machine Intell.*, Vol. 7, pp. 165–177, Feb. 1985.

[59] J.-S. Lee, “Digital image enhancement and noise filtering by use of local statistics,” *IEEE Trans. Pattern Anal. Machine Intell.*, Vol. 2, pp. 165–168, Feb. 1980.

[60] A. Baraldi and F. Parmiggiani, “An Alternative Form of the Lee Filter for Speckle Suppression in SAR Images”, *Graphical Models and Image Processing*, Vol. 57, No. 1, pp. 75–78, Jan.1995.

[61] V. S. Frost, J. A. Stiles, K. S. Shanmugan, J. C. Holtzman, “A Model for Radar Images and its Application to Adaptive Digital Filtering of Multiplicative Noise”, *IEEE Transactions Pattern Analysis and Machine Intelligence*, Vol. PMI-6, No. 5, pp. 658-661, September 1984.

[62] J. W. Woods and J. Biemond, “Comments on ‘A Model for Radar Images and its Application to Adaptive Digital Filtering of Multiplicative Noise’ ”, *IEEE Transactions Pattern Analysis and Machine Intelligence*, Vol. PMI-6, No. 5, pp. 658-661, September 1984.

[63] M. S. Greco and F. Gini, "Statistical Analysis of High-Resolution SAR Ground Clutter Data", *IEEE Transactions on Geoscience and Remote Sensing*, Vol.45, No.3, pp.566-575, March 2007.

[64] A. Lopès, R. Touzi, and E. Nezry, “Adaptive speckle filters and scene heterogeneity,” *IEEE Trans. Geosci. Remote Sensing*, Vol. 28, pp. 992–1000, November 1990.

[65] J.-S. Lee, “Refined filtering of image noise using local statistics”, *Technical report*, Naval Research Laboratory, Washington, DC 20375, January 1980.

[66] A. Lopes, E. Nezry, R. Touzi, and H. Laur, “Structure detection and statistical adaptive speckle filtering in SAR images”, *International Journal of Remote Sensing*, Vol. 14, No. 9, 2010.

[67] A. Buades, B. Coll, and J. M. Morel, “A review of image denoising algorithms, with a new one,” *Multiscale Model. Simul.*, Vol. 4, No. 2, pp. 490–530, 2005.

[68] A. Buades, B. Coll, and J. M. Morel, “Image Denoising Methods. A New Nonlocal Principle”, SIAM Review, Vol. 52, No. 1, pp. 113-147, 2010.

[69] C.-A. Deledalle, L. Denis, and F. Tupin, “Iterative Weighted Maximum Likelihood Denoising With Probabilistic Patch-Based Weights”, *IEEE Trans. Image Proc.*, Vol. 18, pp. 2661–2672, 2009.

[70] F. Argenti and L. Alparone, “Speckle removal from SAR images in the undecimated wavelet domain,” *IEEE Trans. Geosci. Remote Sens.*, Vol. 40, No. 11, pp. 2363–2374, November 2002.

[71] F. Argenti, T. Bianchi, and L. Alparone, “Multiresolution MAP despeckling of SAR images based on locally adaptive generalized Gaussian pdf modeling,” *IEEE Trans. Image Process.*, Vol. 15, No. 11, pp. 3385–3399, November 2006.

[72] P. Perona, and J. Malik, “Scale-Space and Edge Detection Using Anisotropic Diffusion”, *IEEE Transactions On Pattern Analysis and Machine Intelligence*, Vol. 12, No. 7, July 1990.

[73] J. Weickert, “Anisotropic Diffusion in Image Processing”, *ser. ECMI. Stuttgart*, Germany: Teubner, 1998.

[74] L. Alvarez, P.-L. Lions, and J.-M. Morel,“Image Selective Smoothing and Edge Detection by Nonlinear Diffusion II”, *SIAM Journal on Numerical Analysis*, Vol. 29, No. 3, pp. 845-866, June 1992.

[75] Y. Yu and S. Acton, “Speckle reducing anisotropic diffusion,” *IEEE Trans. Image Process.*, Vol. 11, No. 11, pp. 1260–1270, Nov. 2002.

[76] S. Aja-Fernández and C. Alberola-López, “On the estimation of the coefficient of variation for anisotropic diffusion speckle filtering,” *IEEE Trans. Image Processing*, Vol. 15, No. 9, pp. 2694–2701,Sep. 2006.

[77] F. Catté, P. Lions, J. Morel, and T. Coll, “Image selective smoothing and edge detection by nonlinear diffusion,” *SIAM J. Numer. Anal.*, Vol. 29, pp. 182–193, 1992.

[78] J. Weickert, “Coherence-enhancing diffusion filtering,” *Int. J. Comput. Vis.*, Vol. 31, No. 2/3, pp. 111–127, 1999.

[79] N. Nordstrdm, “Biased anisotropic diffusion-A unified regularization and diffusion approach to edge detection”, *Image Vision Comput.*, Vol. 8, No. 4, pp. 318-327, 1990.

[80] F. Torkamani–Azar, K.E. Tait, Image recovery using the anisotropic diffusion equation, *IEEE Trans. Image Proc.*, Vol. 5, 1573–1578, 1996.

[81] G. Gerig, O. Kubler, R. Kikinis. and F.A. Jolesz, “Nonlinear Anisotropic Filtering of MRI Data”, *IEEE Transactions On Medical Imaging.* Vol. 1, No. 2. June 1992.

[82] T. Brox, J. Weickert, B. Burgeth, and P. Mrázek, “Nonlinear structure tensors”, Image and Vision Computing, Vol. 24, No. 1, pp. 41-55, January 2006.

[83] S. Aja-Fernández and C. Alberola-López, “On the estimation of the coefficient of variation for anisotropic diffusion speckle filtering,” *IEEE Trans. Image Processing*, Vol. 15, No. 9, pp. 2694–2701, September 2006.

[84] J. Weickert, B.M. ter Haar Romeny and M.A. Viergever, “Efficient and reliable schemes for nonlinear diffusion filtering”, *IEEE Trans. Image Proc.*, March 1998.